Phase transition of geometrically frustrated TbNiAl in a magnetic field

G. Ehlers
Spallation Neutron Source, Oak Ridge National Laboratory, Building 8600, Oak Ridge, Tennessee 37831-6475, USA

C. Ritter and J. R. Stewart
Institute Laue-Langevin, 6 rue J. Horowitz, 38042 Grenoble, France

A. D. Hillier
ISIS Facility, Rutherford Appleton Laboratory, Chilton, Didcot, Oxon OX11 0QX, United Kingdom

H. Maletta
Hahn-Meitner Institut, Glienicker Strasse 100, 14109 Berlin, Germany

(Received 30 May 2006; revised manuscript received 21 November 2006; published 17 January 2007)

The phase transitions of the geometrically frustrated antiferromagnet TbNiAl in a magnetic field are studied by means of neutron powder diffraction, ac susceptibility, and muon spin relaxation (μSR) measurements. Neutron powder diffraction reveals that, in addition to antiferromagnetic order, ferromagnetic order is induced in a field as low as $B \sim 0.02$ T. At higher fields, ferromagnetic and antiferromagnetic order coexist in different domains in the sample, and the domain balance depends on both magnetic field and temperature. Antiferromagnetic Bragg reflections are observed below a Néel temperature of $T_N = 47$ K which is independent of the field. Ferromagnetic Bragg peaks are observed below a field-dependent Curie temperature which increases from $T_C = 52$ K at $B = 0.2$ T to $T_C = 70$ K at $B = 5$ T. Both phase transitions are concurrently observed in ac susceptibility and μSR measurements.

DOI: 10.1103/PhysRevB.75.024420 PACS number(s): 75.30.Kz, 75.25.+z, 75.50.Ee, 75.50.Cc

I. INTRODUCTION

The ternary intermetallic compounds, in which a rare earth metal is alloyed 1:1:1 with a transition metal and a *p*-electron metal, form a large group and many of such compounds adopt the hexagonal ZrNiAl structure.[1,2] In this structure (space group $P\bar{6}2m$, no. 189) the rare earth site (Wyckoff notation 3*g*) makes a triangular lattice within the *ab* plane which resembles a twisted kagomé lattice (see Fig. 1). The magnetic properties of such compounds[3–5] are often complex and governed by an interplay of strong magnetocrystalline anisotropy, competing near-neighbor interactions, and possibly geometric frustration.[6,7]

TbNiAl is a member of the series which has been studied in detail by means of magnetization, specific heat, ac susceptibility, electrical resistivity measurements, and various neutron scattering techniques.[8–15] In particular, the effect of geometrical frustration on the magnetic properties of TbNiAl in low magnetic fields has become evident in neutron powder diffraction studies. In zero field, a commensurate antiferromagnetic (AFM) propagation vector $\boldsymbol{k}_{\mathrm{AFM}} = (\frac{1}{2}\frac{1}{2}\frac{1}{2})$ is observed. The rare earth lattice position, which has three sites per unit cell, $(x,0,\frac{1}{2})$, $(0,x,\frac{1}{2})$, and $(-x,-x,\frac{1}{2})$ ($x = 0.58$ for TbNiAl), splits into two independent sublattices with different magnetic ordering (see Fig. 1). Two sites out of three per unit cell order with a Néel temperature of $T_N = 47$ K, while the third site is frustrated and acquires a sizable ordered moment only below a second magnetic phase transition at $T_1 = 23$ K. A neutron diffraction experiment with a single-crystal sample in zero field confirmed these findings.[13] Magnetization measurements in applied field revealed a transition to ferromagnetic order in a field of $B = 0.4$ T,[13,14] but neutron diffraction data in a field have not been reported yet to our knowledge.

In zero magnetic field TbNiAl orders as shown in an AFM structure, yet the paramagnetic Curie-Weiss temperature is positive, $\theta_{\mathrm{CW}} \simeq 30$ K,[11] indicating sizable ferromagnetic (FM) correlations between the magnetic moments. Ferromagnetic order in TbNiAl can also be stabilized by applying chemical pressure via Tb-Y or Ni-Cu substitution in the 5% range (but not Ni-Pd substitution).[16–19]

Motivated by these results, we have studied the phase transitions of TbNiAl in a magnetic field, using neutron powder diffraction, ac susceptibility, and muon spin relaxation (μSR) measurements. Our main findings from these experiments, reported in Sec. III, are (1) development of a ferromagnetic phase already at very low fields; (2) increase of the induced ferromagnetic phase with increasing temperature; and (3) increase of ferromagnetic T_C with increasing field.

II. EXPERIMENT

The sample was prepared by inductive levitation melting of the pure elements under argon atmosphere, using 99.99% purity materials or better. X-ray powder diffraction at room temperature confirmed the hexagonal crystal structure.

Neutron diffraction experiments in magnetic fields up to 5 T were performed at the D20 instrument at the Institute Laue-Langevin (ILL). The neutron wavelength was $\lambda = 2.41$ Å. To avoid reorientation of the powder particles in a magnetic field, the sample was immersed in deuterated isopropanol. Isopropanol freezes around $T \sim 115$ K in a glassy state, giving rise to a weak and broad bump in the data around $2\theta = 35°$ ($Q \sim 1.6$ Å^{-1}). After initial rapid cooling of

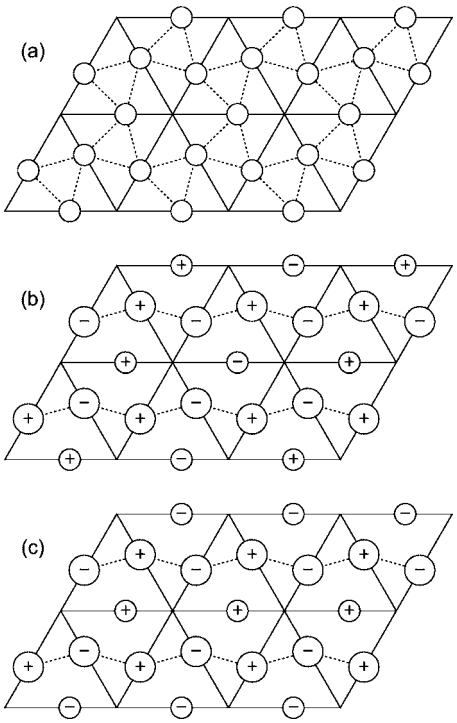

FIG. 1. (a) Lattice made up by the R site in one ab plane in the ZrNiAl structure. Magnetic order observed in TbNiAl below T_1 (b) and in the temperature range $T_1 \leq T \leq T_N$ (c). Smaller circles represent frustrated moments, which have a lower but nonzero time-averaged value.

the sample in the remanent field of the magnet, during the experiment the temperature was never raised above the glass transition temperature of isopropanol. It was therefore guaranteed that the powder remained fixed and that the same powder average was measured in each run. In subsequent runs the sample was cooled to base temperature in different fields and diffraction patterns were measured during slow warming of the sample (typically 6 h to reach $T \sim 70$ K).

Since the cryogenic equipment created a large instrument background, analysis of the magnetically ordered phases was primarily performed using diffraction patterns where a high-temperature pattern from the paramagnetic phase was subtracted for each field. This left only the temperature-dependent magnetic Bragg peaks in the pattern. The patterns were refined using the FULLPROF package.[20] The scale factor for the refinement cannot be reliably determined from a difference pattern and was therefore calculated using unobstructed Bragg peaks from a data set measured in the paramagnetic phase. Values for magnetic moments that will be quoted below account for the resulting uncertainty of the scale factor.

Susceptibility measurements were performed at Hahn-Meitner Institut (HMI) using a fully calibrated Lake Shore ac susceptometer (model 7221) that allowed measurements above liquid helium temperature, in superimposed dc fields up to 1 T. The powder was again fixed with nonmagnetic glue to assure that no reorientation of the grains affected the results.

Zero-field (ZF) and longitudinal-field (LF) μSR measurements were performed using the MuSR muon spectrometer

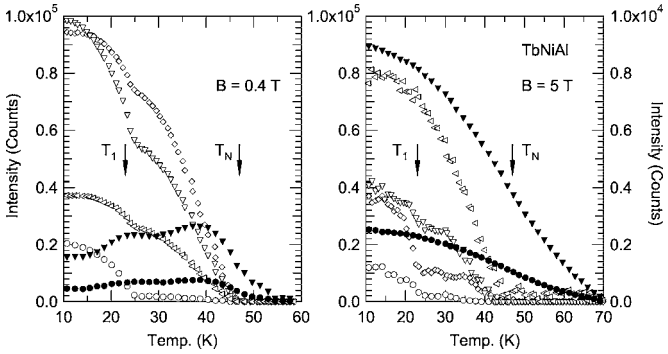

FIG. 2. Magnetic Bragg peaks of TbNiAl observed in a field of $B=0.4$ T (left panel) and $B=5$ T (right panel). Integer hkl are shown in full symbols: ●=(100) and ▼=(110). Half-integer hkl are shown with open symbols: ○=(1/2,−1/2,1/2), ◇=(1/2,1/2,1/2), ▽=(3/2,−1/2,1/2), and ◁=(3/2,−3/2,1/2). Note that in the right panel the half-integer peaks are scaled to the right axis which is blown up by a factor of 10.

at the ISIS muon facility, Didcot, U.K. The muons were implanted in a 30-mm-diameter, 1-mm-thick powder sample mounted in a silver sample holder. This ensured that any muons implanted around the sample did not contribute to the measured muon relaxation spectrum. The muons come to rest in the sample and precess around the internal field at the muon site. Each muon subsequently decays into a positron which is preferentially emitted along the muon spin direction. The resulting positron is detected, time stamped, and collected into histograms of the positron counts $N_F(t)$ and $N_B(t)$ in the forward and backward grouping of the detectors. Using these histograms, the time evolution of the muon polarization is measured.

The muon spin relaxation spectra $G_z(t)$ are obtained from the positron histograms. After correcting for the dead time of each detector, $G_z(t)$ is extracted from the ratio of the forward and backward detectors:

$$P(t) = a_0 G_z(t) = \frac{N_F(t) - \alpha N_B(t)}{N_F(t) + \alpha N_B(t)}, \tag{1}$$

where a_0 is the initial asymmetry and α is a normalization constant to account for the varying efficiencies of the forward and backward detectors. Measurements were collected (after zero-field cooling the sample down to 12 K) upon warming the sample from 12 to 150 K.

III. RESULTS

A. Neutron diffraction

Figure 2 shows, as an example, the magnetic Bragg peaks of TbNiAl as observed in fields of $B=0.4$, and 5 T. The most important observation from neutron powder diffraction is that Bragg peaks with both half-integer and integer hkl indices appear in the same patterns for all fields between $B=0.02$ and 5 T.

The occurrence of both types of magnetic peaks can have two possible origins leading at the atomic level to identical structure factors: the field either (i) drives the system ferri-

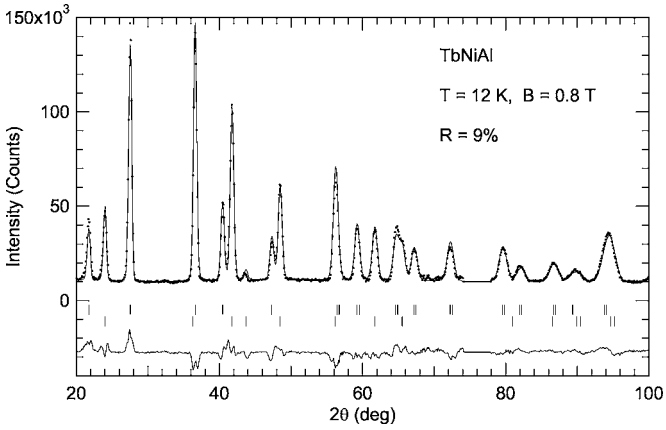

FIG. 3. Refined difference diffraction pattern of TbNiAl at $T=12$ K, $B=0.8$ T. Upper and lower rows of reflection markers correspond to Bragg peak positions with half-integer and integer *hkl* indices, respectively.

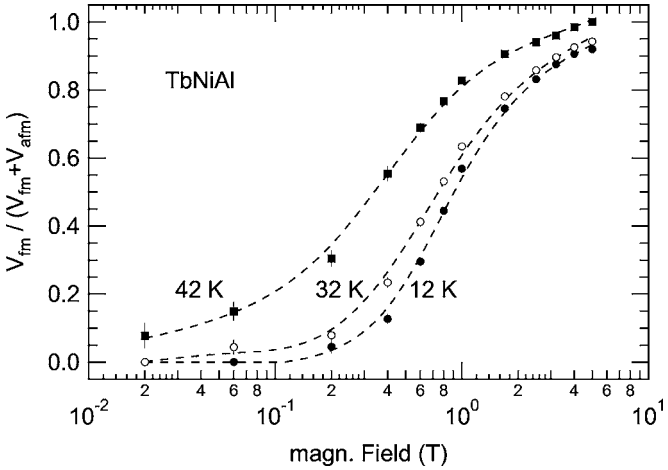

FIG. 4. Volume fraction of ferromagnetic domains with respect to the sum of ferro- and antiferromagnetically ordered volume, observed in TbNiAl at $T=12$, 32, and 42 K.

magnetic, or (ii) into a coexistence of AFM and FM ordered domains. The first scenario can be ruled out as the refinement leads for one of the sublattices to an unphysical high value of the magnetic moment at low temperature. For example, in the refinement of Fig. 3 at $B=0.8$ T and $T=12$ K, a ferrimagnetic model results in values for the ordered moments in the two sublattices of $\mu_1=(11.2\pm0.1)\mu_B$ and $\mu_2=(-0.6\pm0.1)\mu_B$. For comparison, the $^7F_6$ ground state of the Tb^{3+} ion ($L=S=3$) can obtain a moment no larger than $g_J J=9\mu_B$. If, on the other hand, it is assumed that different domains exist and that the ordered moment in both types of domains is the same, a volume ratio of AFM to FM domains of 55:45 results in an ordered moment of $\mu=(8.0\pm0.1)\mu_B$.

To study the field and temperature dependence of the ratio between the two volume fractions, a model was used which assumes that the *c* axis remains the easy magnetization axis in TbNiAl as well in the ferromagnetic state: This assumption is consistent with the observed relative intensities of the FM peaks below $B\sim4$ T, and with the apparent absence of a magnetic (001) reflection. The AFM order was assumed to be identical to the one found in zero field. With the additional assumption that the ordered moment is always the same in both types of domains (unfrustrated moments for the AFM phase) the respective volume fractions of FM and AFM domains can be determined from the intensities of the integer (FM) and half-integer (AFM) *hkl* peaks in the difference patterns as a function of *B* and *T*. This analysis then also yields the magnitudes of the ordered magnetic moments, which are found consistent with earlier neutron diffraction results in zero magnetic field, around $8\mu_B$ at base temperature (at higher temperature the ordered moments become smaller).[9,13] The size of the 33% frustrated moments in the AFM domains is a free parameter in the refinements, and at temperatures above T_1 these moments are always found very small (below $\sim1\mu_B$).

Below $B\sim4$ T, the resulting magnetic *R* factors are generally between 5% and 10%, indicating that with such a model one obtains a reasonable description, but does not account for all details of the resulting local moment structure in the field (see the discussion below on the influence of the magnetic anisotropy). At the highest fields in our study a weak (001) peak occurs and overall the magnetic *R* factors of the refinements become larger, indicating that the model starts to break down. At $B=5$ T the field is already able to partly overcome the magnetocrystalline anisotropy which tends to align the ordered spins in a direction parallel to the *c* axis (this applies to the grains that are orientated with the *c* axis not parallel to the field).

The temperature dependence of the FM peaks remarkably shows that, in magnetic fields below $B\sim0.8$ T, they increase in intensity as temperature is increased up to about $T=42$ K. This indicates that the balance between near-neighbor AFM and FM couplings in a field is very fragile and depends on temperature, and that generally AFM domains turn into FM domains as temperature is raised. This remarkable result is shown in Fig. 4 where the field dependence of the FM volume fraction is given for different temperatures. A field of 200 G is sufficient to induce some ferromagnetism, while in zero field several studies have not reported any ferromagnetism at all.[11,13] The gradual transition to FM order with increasing field is observed in both AFM phases above and below T_1.

At all fields, AFM peaks are observed only below $T_N=47$ K which is rather insensitive to the field (apparent change with the field less than 1 K). The Curie temperature, however, defined as the critical temperature below which FM Bragg peaks are observed, increases from $T_C=52$ K at $B=0.2$ T to $T_C=70$ K at $B=5$ T. Therefore, above 47 K in a field, TbNiAl (powder) is in parts ferromagnetic and paramagnetic, ferromagnetic order being preferentially present in grains whose *c* axis is aligned close to parallel to the field direction.

B. ac susceptibility

The results of susceptibility measurements are summarized in Fig. 5. In zero field the real part of the ac susceptibility has its maximum above the Néel temperature, at $T=47.5$ K.[21] In applied field the peak moves to lower tem-

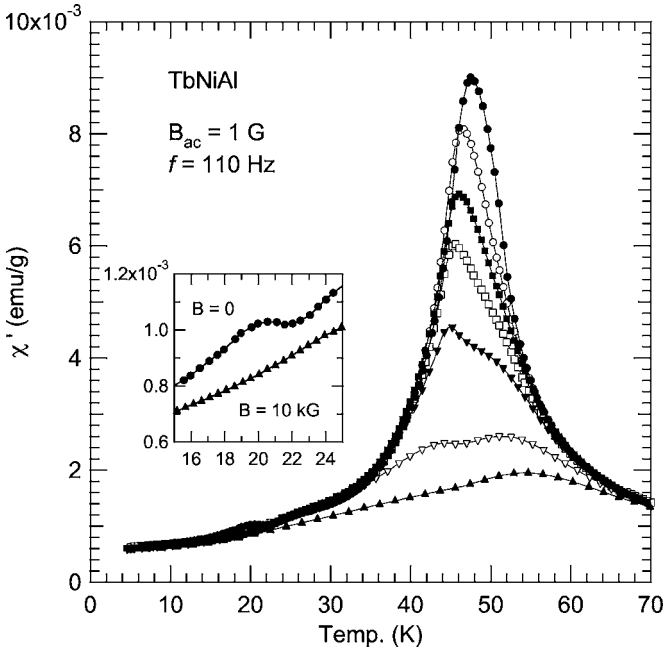

FIG. 5. The real part of the ac susceptibility in applied field: (●) 0, (○) 0.1, (■) 0.15, (□) 0.2, (▼) 0.3, (▽) 0.5, and (▲) 1 T.

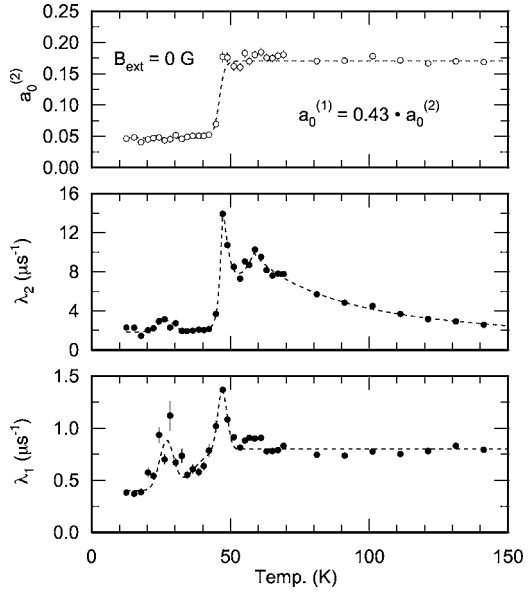

FIG. 6. Muon relaxation rates λ_1, λ_2 and asymmetries $a_0^{(1)}$, $a_0^{(2)}$ in zero magnetic field. Maxima are observed at 27, 47, and 58 K. Lines are guides to the eye.

perature. The phase transition at $T_1=23$ K is observable as a weak anomaly which becomes invisible in an applied field as low as 0.1 T (see inset of Fig. 5) whereas neutron diffraction reveals that the transition still exists at the highest fields (see right-hand panel in Fig. 2). As the field rises, a shoulder to the high-temperature side of the peak appears, which develops into a second peak that becomes clearly visible in a field of $B=0.3$ T and higher. The second peak is a clear signature of a ferromagnetic phase transition. This peak moves to higher temperature as the field is increased, but not exactly like the Curie temperature observed in neutron diffraction. For example, at the highest field ($B=1$ T), the peak in ac susceptibility occurs at $T=54.2$ K while at this field FM Bragg peaks occur up to $T=63$ K. The difference between the two techniques that causes the apparent disconnect in the observed temperature evolution of the critical temperatures is that with ac susceptibility one measures a volume average of the sample whereas with neutron diffraction one is sensitive to the grains with the highest local T_C which may depend on the orientation with respect to the field.

C. Muon spin relaxation

Quasielastic neutron scattering experiments (NSEs) revealed that, in the intermediate temperature range $T_1 \leq T \leq T_N$, the frustrated spins in TbNiAl retain a large paramagnetic component.[15] This was shown by analysis of the quasielastic diffuse scattering of neutrons at temperatures above T_1. The spin dynamics is Q independent and single exponential in time, with characteristic relaxation times τ ranging from 0.01 to 0.1 ns, depending on temperature.

The ZF μSR results are summarized in Fig. 6. The line shape $P(t)$ of the muon relaxation can be very well described by a double exponential

$$P(t) = a_0^{(1)}\exp(-\lambda_1 t) + a_0^{(2)}\exp(-\lambda_2 t) + C \qquad (2)$$

with a time-independent background C, two muon relaxation rates $\lambda_{1,2}$, and a constant ratio of the two corresponding asymmetries $a_0^{(1)}$, $a_0^{(2)}$. Hence this is consistent with the NSE result and indicates that the muons stop in two different interstitial sites with different magnetic fields. The magnitude of these fields can be estimated via $\lambda=2\Delta^2\tau$ where the local time-averaged second moment of the field is $\Delta^2=\gamma_\mu^2\langle B^2\rangle$ ($\gamma_\mu/2\pi=13.55$ MHz/kG is the muon gyromagnetic ratio).[22] In the paramagnetic phase this results in $\sqrt{\langle B^2\rangle}\simeq 40$ kG for site 1 and $\sqrt{\langle B^2\rangle}\simeq 90$ kG for site 2. The transition at $T=47$ K is clearly identified in the data as magnetic ordering. The drop in asymmetry at lower temperature is due to a strong muon depolarization that takes place immediately when the muon enters the sample. Interestingly, a third maximum of the relaxation rates λ is found at $T=58$ K, which does not correspond to a phase transition observable with neutron diffraction.

LF μSR in an applied field of $B=0.25$ T gives essentially the same result (Fig. 7). Clearly, two phase transitions are still observed in the field, which are somewhat broadened in temperature. The transition temperatures are shifted to slightly higher values, which is consistent with ac susceptibility. The high-temperature maximum at 58 K can in this case be identified with the ferromagnetic phase transition and its broad appearance confirms the local differences in T_C in different domains of the sample.

IV. DISCUSSION

In summary, a fragile balance between near-neighbor AFM and FM couplings is found in TbNiAl in a magnetic field. To some extent, the details of the particular metamagnetic transition described here are due to the sample being a

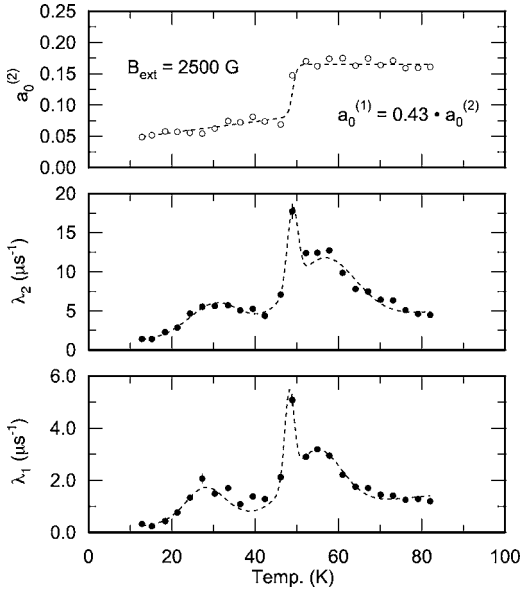

FIG. 7. Muon relaxation rates λ_1, λ_2 and asymmetries $a_0^{(1)}$, $a_0^{(2)}$ in an applied magnetic field of $B=2500$ G. Maxima are observed at 29, 49, and 56 K. Lines are guides to the eye.

powder. Grains that differ in their alignment with respect to the field direction are likely to respond differently to the field. While the single-crystal study by Javorský *et al.*[13] has shown that the *c* axis is clearly the easy magnetization axis, it is not known how the critical field and temperature for a switch to FM order in a single-monocrystal domain depend on the direction of the field relative to the crystal axes. However, even the lowest applied field of 0.02 T is able to drive parts of the system ferromagnetic. The observed strong increase of T_C with applied magnetic field also indicates the strong influence of the field in promoting the existing ferromagnetic exchange interactions.

In zero field TbNiAl has two different magnetic phases and a transition temperature $T_1=23$ K. Both these phases are observed in applied field as well and the temperature T_1 remains unchanged up to $B=5$ T.

The dynamic techniques, ac susceptibility and μSR, have given results that are mostly consistent with the neutron diffraction results. μSR picked up a precursor to the ferromagnetic phase transition even in zero field at a temperature where neutron scattering does only see a paramagnetic state. Further neutron scattering studies using a single-crystal sample are necessary to obtain significantly better insight into this transition. In a single-crystal study one expects the observed transitions to be sharper, and the well-defined field direction should lead to a less pronounced coexistence of FM and AFM domains.

ACKNOWLEDGMENTS

The authors would like to thank F. Thomas (ILL) for his help in setting up the magnetic field equipment in the neutron scattering experiments. This work is supported by the Spallation Neutron Source Project (SNS). SNS is managed by UT-Battelle, LLC, under Contract No. DE-AC05-00OR22725 for the U.S. Department of Energy (DOE).

[1] A. E. Dwight, M. H. Mueller, R. A. Conner, J. W. Downey, and H. Knott, Trans. Metall. Soc. AIME **242**, 2075 (1968).
[2] E. Parthé and B. Chabot, in *Handbook of the Physics and Chemistry of Rare Earths*, edited by K. A. Gschneidner, Jr. and L. Eyring (Elsevier, Amsterdam, 1984), Chap. 48, p. 113.
[3] H. Oesterreicher, J. Less-Common Met. **30**, 225 (1973).
[4] A. Szytuła, *Crystal Structures and Magnetic Properties of RTX Rare Earth Intermetallics* (Jagiellonian University Press, Kraków, 1998).
[5] A. Szytuła, in *Handbook of Magnetic Materials*, edited by K. H. J. Buschow (Elsevier, Amsterdam, 1991), Vol. 6, p. 85.
[6] A. P. Ramirez, Annu. Rev. Mater. Sci. **24**, 453 (1994); in *Handbook of Magnetic Materials*, edited by K. H. J. Buschow (Elsevier, Amsterdam, 2001), Vol. 13, Chap. 4.
[7] *Frustrated Spin Systems*, edited by H. T. Diep (World Scientific, Singapore, 2004).
[8] N. C. Tuan, Ph.D. thesis, Charles University, Prague, 1992.
[9] H. Maletta and V. Sechovský, J. Alloys Compd. **207-208**, 254 (1994).
[10] P. Javorský, N. C. Tuan, M. Diviš, L. Havela, P. Svoboda, V. Sechovský, and G. Hilscher, J. Magn. Magn. Mater. **140-144**, 1139 (1995).
[11] G. Ehlers and H. Maletta, Z. Phys. B: Condens. Matter **99**, 145 (1996).
[12] G. Ehlers, Ph.D. thesis, Technical University, Berlin, 1996.
[13] P. Javorský, P. Burlet, V. Sechovský, A. V. Andreev, J. Brown, and P. Svoboda, J. Magn. Magn. Mater. **166**, 133 (1997).
[14] N. K. Singh, K. G. Suresh, R. Nirmala, A. K. Nigam, and S. K. Malik, J. Magn. Magn. Mater. **302**, 302 (2006).
[15] G. Ehlers, H. Casalta, R. E. Lechner, and H. Maletta, Phys. Rev. B **63**, 224407 (2001).
[16] G. Ehlers, C. Ritter, A. Krutjakow, W. Miekeley, N. Stüßer, Th. Zeiske, and H. Maletta, Phys. Rev. B **59**, 8821 (1999).
[17] H. Kitazawa, S. Eguchi, G. Kido, and G. Cao, J. Alloys Compd. **408-412**, 58 (2006).
[18] G. Ehlers, D. Ahlert, C. Ritter, W. Miekeley, and H. Maletta, Europhys. Lett. **37**, 269 (1997).
[19] H. Kitazawa, S. Eguchi, and G. Kido, Physica B **329-333**, 1053 (2003).
[20] J. Rodriguez-Carvajal, Physica B **192**, 55 (1993).
[21] M. E. Fisher, Philos. Mag. **7**, 1731 (1962).
[22] A. Keren, P. Mendels, I. A. Campbell, and J. Lord, Phys. Rev. Lett. **77**, 1386 (1996).